

Flight and Ground Results from Long-Wave and Mid-Wave Airborne Hyperspectral Spectrographic Imagers

Stephen Achal^a, John E. McFee^b and Douglas Davison^a

^a Itres Research Limited, Suite 110 3553 31 St. NW, Calgary, AB, Canada T2L2K7

^b Defence R&D Canada Suffield, Box 4000, Station Main, Medicine Hat, AB, Canada, T1A 8K6

Abstract

Wide-swath LWIR and MWIR airborne pushbroom hyperspectral imagers based on efficient optics, cryo-cooled custom MCT FPAs and fast, quiet readout electronics have been developed and are in commercial production. First-light and first-flight images from the LWIR airborne hyperspectral imager (TASI) and MWIR hyperspectral imager (MASI) were acquired in summer 2006 and summer 2008 respectively. The TASI and MASI systems meet, and in some cases exceeded, the original design specifications. TASI systems have been successfully involved in worldwide applications ranging from systematic buried landmine detection research to large-scale high-resolution aerial mapping for geological exploration. The MASI, being a relative newcomer to commercial aerial applications, has found utility in large-scale targeted geological surveys.

1.0 Introduction

DRDC Suffield and Itres Research have collaborated to investigate the use of passive pushbroom hyperspectral imaging for surface and buried landmine detection since 1989. As an outcome of that program, Itres designs, develops, operates and markets a family of hyperspectral pushbroom imagers which are ideally suited for landmine detection, but which also have numerous applications outside the defence community. The visible/near infrared (UV/VNIR, 380 to 1050 nm wavelength) hyperspectral imager has demonstrated a high probability of detection and low false alarm rate for daytime passive detection of surface-laid mines, based on pattern classification of their reflectance spectra, from airborne and ground-based platforms, independent of angle of illumination caused by time of day, season and geography.¹ The short-wave infrared (SWIR, 950 to 2450 nm wavelength) hyperspectral imager has demonstrated the ability to discriminate classes of materials associated with surface mines, other threat objects and natural backgrounds, independent of their visible band colour.² The TASI thermal or long-wave infrared (LWIR, 8000 to 11500 nm wavelength) has demonstrated the ability to detect buried objects and can characterize certain gaseous materials.³ In preliminary studies performed in summer 2007, all three had shown promise to detect surface improvised explosive devices (IEDs). To date, the MASI mid-wave infrared hyperspectral imager (MWIR, 3000 to 5000nm) has been limited to geological surveys. Intriguingly, the authors have been able to generically isolate anthropogenic material in day/night data.

2.0 LWIR hyperspectral Imager (TASI)

The TASI's optical train is a diffraction-limited, all-refractive, un-cooled, prism-based f/1.5 imaging spectrograph. The spectrograph is coupled to a cryogenically-cooled MCT array. This combination produces a total FOV of 40 degrees across 600 spatial pixels and a spectral range of 8.0 to 11.5 μ m across 32 bands. The spectral smile and keystone distortion are less than 0.5 pixels. The MCT readout produces low noise 14-bit data at a rate of 5 Mpixels/s. The dimensions of the spectrograph head are 30 cm (w) by 85 cm (h) by 20 cm and its mass is 40 kg (see figure 1). TASI is designed to operate in most light aircraft environments, as well as from ground-based vehicle platforms. It can be combined with

Flight and Ground Results from Long-Wave and Mid-Wave Airborne Hyperspectral Spectrographic Imagers



Figure 1: TASI hyperspectral imager sensor head mounted in a fixed-wing aircraft

INS/DGPS to produce ortho-rectified data products which can be mosaicked. In addition, TASI is fully compatible with the Itres real-time processing system⁴ which is capable of real-time data backup, radiometric calibration, diagnostics alerts, image processing and target detection.

Figure 2 shows a graph of the radiant sensitivity of the imager versus wavelength and illustrates response across 8000 to 12000 nm. The typical noise floor, system gain and full well of the FPA were determined to be 2200 electrons, 2300 electrons/DN and 34 million electrons respectively. Figure 3 shows a graph of the NE Δ T of the imager versus wavelength at 300K and 1.0 m spatial resolution. The sensitivity across most of the band is seen to be better than 0.2K, which is acceptable for landmine detection applications.

First-light images were obtained in summer 2006 (see figure 4). As an illustration of the ability of TASI to discriminate different materials, Figure 5 shows a three band visible wavelength image of a person spraying tetrafluoroethane (Dust-OffTM). Although the spray cans are clearly visible, the tetrafluoroethane is invisible. A three band image taken with the TASI imager (Figure 6) clearly highlights the tetrafluoroethane as two red clouds. The colour indicates that the emissivity of the cloud differs in the three bands and thus identification of a material is feasible based on band selection or other appropriate spectral classification techniques. Of further interest is the vegetation in the scene, which appears uniformly grey, regardless of species or health (several of the deciduous trees were in various stages of senescence). This implies that vegetation has equal reflectivity across all bands of the thermal infrared (i.e., is "colourless"), which would make it readily separable from other materials.

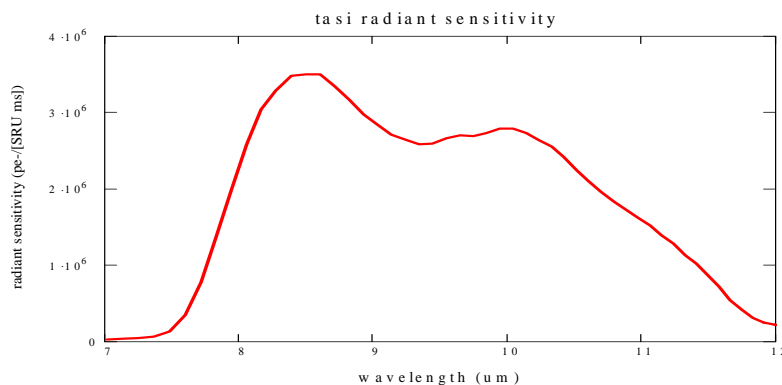


Figure 2: TASI radiant sensitivity versus wavelength

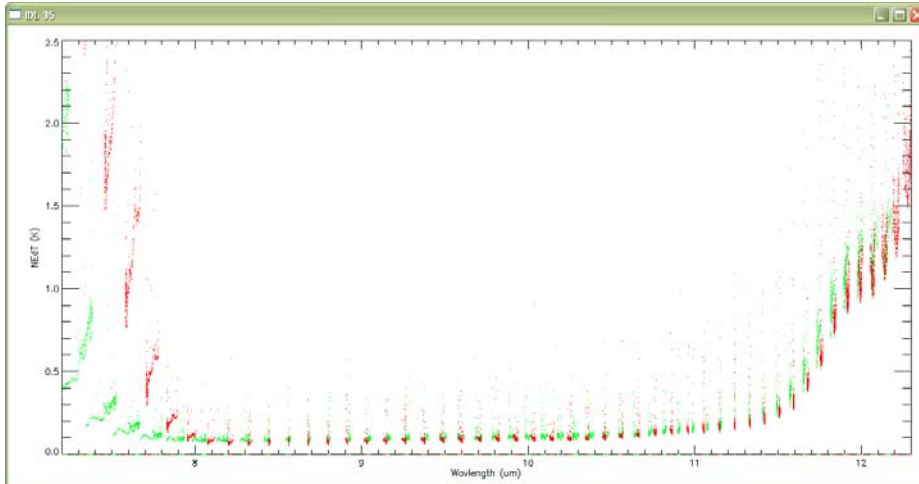


Figure 3: *NEdT vs. wavelength, 300K blackbody*



Figure 4: *TASI First-Light image*



Figure 5

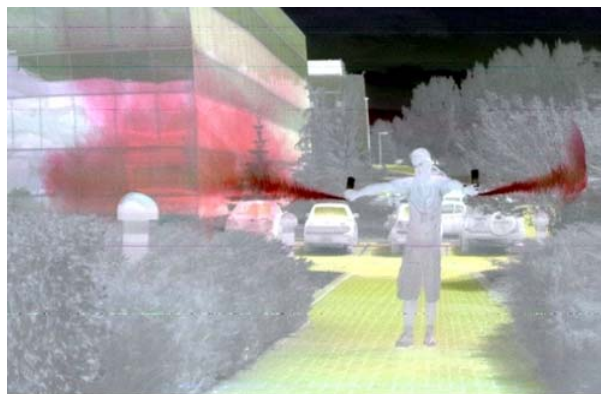


Figure 6

Figures 5 and 6: *Image of person spraying tetrauroethane gas, taken with visible three band imager (left image). The gas is invisible. Three band image of person spraying tetrauroethane, taken with TASI at the same time as Figure 5. Two clouds of gas (red) are visible.*

Figures 7 and 8 illustrate the ability of a TIR hyperspectral imager to detect and distinguish materials from an airborne platform. Figure 7 is an aerial image of a sulfur recovery plant near Calgary taken with visible band imager. Emission from the smokestack is invisible. Figure 8 is an aerial image of the same sulfur recovery plant as Figure 7 taken at the same time with TASI. Emission from the smokestack is clearly visible as a plume which has red and white parts. The red colour is again indicative of non-uniform emissivity across the thermal band. The full spectrum can be used to help

Flight and Ground Results from Long-Wave and Mid-Wave Airborne Hyperspectral Spectrographic Imagers

identify the composition of the gas. Figure 9 is another example of how anthropogenic materials may be differentiable by chemical composition as well as temperature using a TIR hyperspectral imager. It is an orthorectified three band false colour image taken by TASI over the city of Calgary, Canada. In the colour image the dome of the oval building appears orange, whereas it is white in the visible band. The non-uniform emissivity across the band is related to the specific materials used in the dome fabric. It is also possible to distinguish non-anthropogenic materials and geological features using this approach.



Figure 7



Figure 8

Aerial image of a sulfur recovery plant near Calgary taken with visible band imager. Emission from smokestack is not visible in the left image. Figure 8 shows a non-orthorectified TASI aerial image of the same sulfur recovery plant acquired at the same time as Figure 7. In this three band false colour image, emission from the smokestack is clearly visible as an orange and white plume.



Figure 9: Three band colour composite of an orthorectified TASI image over Calgary AB.

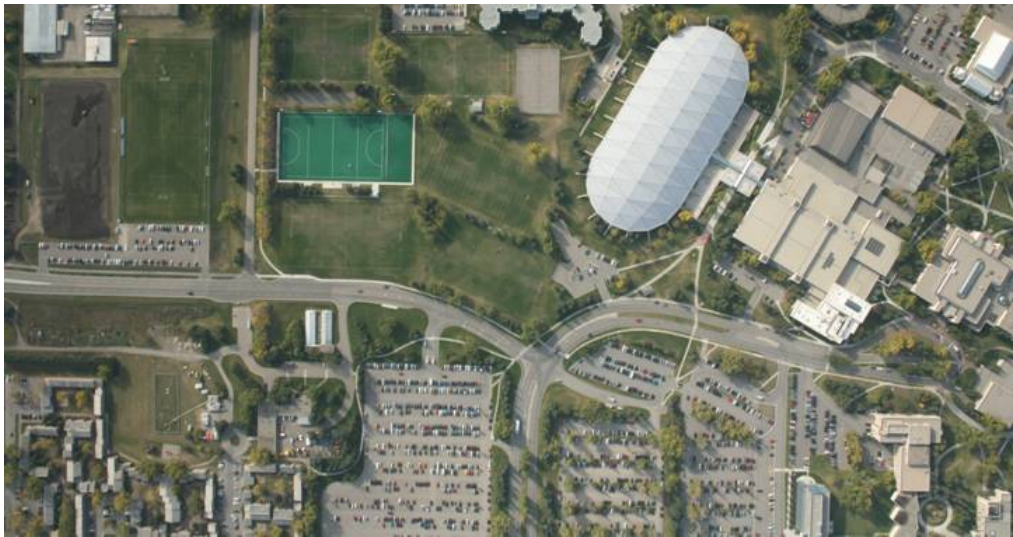


Figure 10: Visible spectrum aerial image taken at the same as the TASI image in Figure 9.

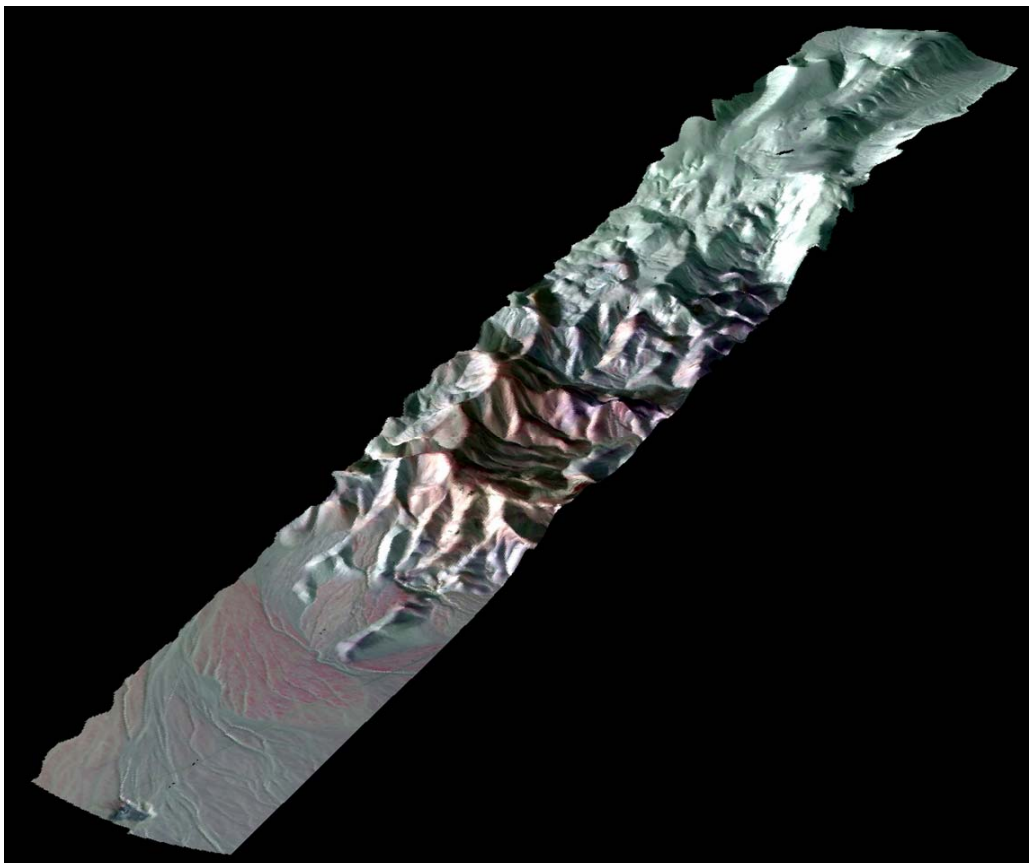


Figure 11: Orthorectified TASI image of a site near Cuprite, Nevada

Figure 10 shows a visible image acquired at the same time as the TASI image in figure 9. A comparisons between the two images reveals interesting features uniquely visible in the hyperspectral LWIR and visible. Figure 11 shows a typical geological mapping TASI product. In the figure, 2m TASI orthorectified data of a site near Cuprite, Nevada is draped over a digital elevation model. The various surface-exposed minerals show as various shades of red and green. The TASI image strip is 1.2km wide and 12km long.

Flight and Ground Results from Long-Wave and Mid-Wave Airborne Hyperspectral Spectrographic Imagers

3.0 MWIR hyperspectral Imager (MASI)

The MASI's optical train is a diffraction-limited, all-refractive, un-cooled, prism-based $f/2.0$ imaging spectrograph. The spectrograph is coupled to a cryogenically-cooled MCT array. This combination produces a total FOV of 40 degrees across 640 spatial pixels and a spectral range of 3.0 to 5.0 μm across 64 bands. The spectral smile and keystone distortion are less than 0.5 pixels. The MCT readout produces low noise 14-bit data at a rate of 5 Mpixels/s. The dimensions of the spectrograph head are 37.9 cm (w) by 73.4 cm (h) by 18.3 cm (l) and its mass is 20 kg (see figure 12). MASI, like TASI, is designed to operate in most light aircraft environments, as well as from ground-based vehicle platforms. It can be synchronized with INS/DGPS to produce orthorectified data products which can be mosaicked. In addition, MASI is fully compatible with the Itres real-time processing system⁴ which is capable of real-time data backup, radiometric calibration, diagnostics alerts, image processing and target detection.

The typical noise floor, system gain and full well of the FPA were determined to be 2400 electrons, 1150 electrons/DN and 18 million electrons respectively. Figure 13 shows a graph of the NEdT of the imager versus wavelength at 300K and 1.0 m spatial resolution. The sensitivity across most of the band is seen to be better than 0.2K. The increase in NEdT values below 3.75 μm and above 4.90 μm are due to the very low spectral radiance of a 300K blackbody and the cold-filter's 4.85 μm spectral cut-off respectively.



Figure 12: MASI hyperspectral imager sensor head mounted in a fixed-wing aircraft

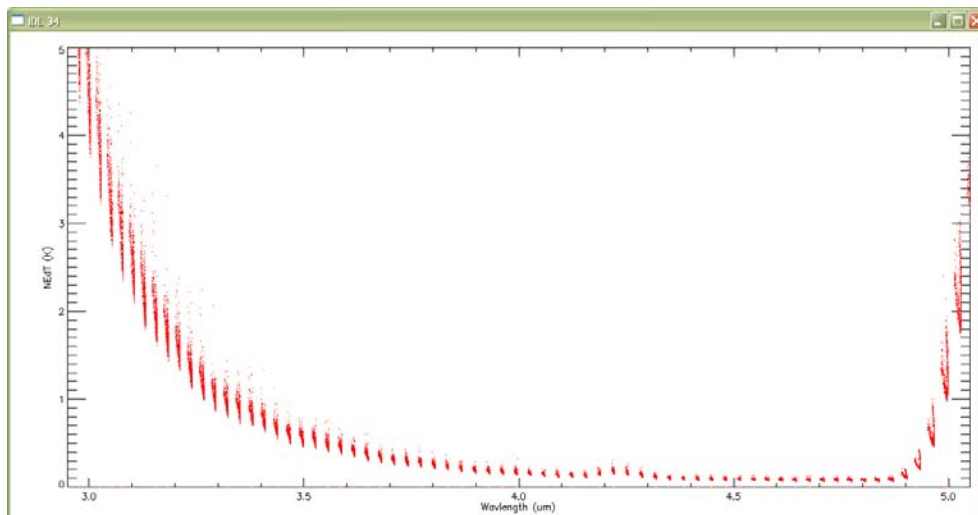


Figure 13: NEdT vs. wavelength, 300K blackbody

Flight and Ground Results from Long-Wave and Mid-Wave Airborne Hyperspectral Spectrographic Imagers

First-flight images were obtained in September 2008 over Black Diamond, Alberta (near Calgary). MASI's real-time display screen is shown in figure 14. Five north-south and three east-west lines were flown (see figure 15). Each line was 5 km long. The orthogonal flight lines facilitated the computation of the bundle-adjustment parameters and subsequent image mosaicking. The average ground speed and altitude were 110 knots and 700 meters above ground. This resulted in an average ground resolution of 1.0m/pixel. The flight data were collected at 9AM under overcast skies... very low solar spectral radiance!



Figure 14: MASI's real-time waterfall display



Figure 15: MASI's first test flight plan on Google Earth data

Figure 16 that follows shows the first MASI airborne image (red: 3571nm, green: 3952nm, blue: 4778nm). Anthropogenic materials are differentiable by chemical composition as well as temperature, similar to the TASI.

Flight and Ground Results from Long-Wave and Mid-Wave Airborne Hyperspectral Spectrographic Imagers



Figure 16: *MASI's first airborne data*

The orthorectified mosaic of MASI flight lines created during bundle adjustment evaluation is shown in Figure 17. In this figure, the result of changing ground spectra based on the time of acquisition of each flight line can be seen. For example, the first line acquired was the westernmost north-south flight line seen towards the left side of the image. Ground temperatures increased with each subsequent line. Hence, the radiance of each succeeding flight line also increased. Ground temperatures 'stabilized' at 10°C during the collection of the east-west lines.

Note that the diamond shaped patterns seen in Figure 17 relate to the orthocorrection of the two orthogonal sets of flight lines (the brighter east-west flight lines and darker north-south lines). This is part of our internal evaluation procedure and is avoided during production processing.



Figure 17: *Orthorectified MASI mosaic of the flight data*

4.0 Conclusion and Future Developments

This paper briefly described some of the exciting results generated from MASI's and TASI's first-light and first-flights. Since their inaugural first-flights, MASI and TASI have become established and versatile commercial-off-the-shelf infrared hyperspectral imaging systems. They are showcasing the utility of using high spatial resolution hyperspectral infrared for a large variety of applications ranging

from humanitarian endeavors to extremely large-scale commercial aerial surveys. The next generation MASI and TASI systems will continue to fulfill the ongoing need for faster, more sensitive and higher spatial resolution systems required in emerging commercial and military infrared hyperspectral applications markets.

References

1. J.E.McFee, C.D.Anger, S.B.Achal, and T.Ivanco, "Land mine detection using passive hyperspectral imaging," in *Chemical and Biological Sensing VIII*, A.W.Fountain III, ed., Proceedings of SPIE 6554, April 2007.
2. J.E.McFee, S.B.Achal, T.Ivanco, and C.Anger, "A shortwave infrared hyperspectral imager for landmine detection," in *Detection and Remediation Technologies for Mines and Mine-like Targets X*, R.S.Harmon, J.T.Broach, and J.H.Holloway, eds., Proceedings of SPIE 5794, pp. 56–67, April 2005.
3. S.B.Achal, J.E.McFee, T.Ivanco, and C.Anger, "A thermal hyperspectral imager (TASI) for buried land mine detection," in *Detection and Remediation Technologies for Mines and Mine-like Targets XII*, R.S.Harmon, J.T.Broach, and J.H.Holloway, eds., Proceedings of SPIE 6553, April 2007.
4. T.Ivanco, S.B.Achal, J.E.McFee, C.D.Anger, and J.Young, "Real-time airborne hyperspectral imaging of land mines," in *Detection and Remediation Technologies for Mines and Mine-Like Targets XII*, R.S.Harmon, J.T.Broach, and J.H.Holloway, eds., Proceedings of SPIE 6553, April 2007.

**Flight and Ground Results from Long-Wave and
Mid-Wave Airborne Hyperspectral Spectrographic Imagers**

